Strain-Engineered Ferroelastic Structures in $PbTiO_3$ Films and their Control by Electric Fields

Eric Langenberg[1,], Hanjong Paik[1], Eva H. Smith[1], Hari P. Nair[1], Isabelle Hanke[2], Steffen Ganschow[2], Gustau Catalan[3], Neus Domingo[3], Darrell G. Schlom[1,4,*]*

[1]Department of Materials Science and Engineering, Cornell University, Ithaca, New York 14853, USA.

[2]Leibniz-Institut für Kristallzüchtung, Max-Born-Straße 2, 12489 Berlin, Germany

[3]Catalan Institute of Nanoscience and Nanotechnology (ICN2), CSIC, Barcelona Institute of Science and Technology, Campus Universitat Autònoma de Barcelona, Bellaterra, 08193 Barcelona, Spain.

[4]Kavli Institute at Cornell for Nanoscale Science, Ithaca, New York 14853, USA.

Abstract:

We study the interplay between epitaxial strain, film thickness, and electric field in the creation, modification, and design of distinct ferroelastic structures in $PbTiO_3$ thin films. Strain and thickness greatly affect the structures formed, providing a two-variable parameterization of the resulting self assembly. Under applied electric fields these strain-engineered ferroelastic structures are highly malleable, especially when *a*/*c* and a_1/a_2 superdomains coexist. To reconfigure the ferroelastic structures and achieve self-assembled nanoscale-ordered morphologies, pure ferroelectric switching of individual *c*-domains within the *a*/*c* superdomains is essential. The stability, however, of the electrically written ferroelastic structures is in most cases ephemeral; the speed of the relaxation process depends sensitively on strain and thickness. Only under low tensile strain—as is the case for $PbTiO_3$ on $GdScO_3$—and below a critical thickness do the electrically created *a*/*c* superdomain structures become stable for days or longer, making them relevant for reconfigurable nanoscale electronics or non-volatile electromechanical applications.

KEYWORDS: $PbTiO_3$ films, Ferroelastic switching, strain engineering, piezoresponse force microscopy, stability of ferroelastic structures.

INTRODUCTION

Ferroelastic structures, many of them formed by ferroelectric-ferroelastic domain architectures, have attracted significant attention in the last few years.[1–6] On the one hand, the polar character of the ferroelectric domains has promoted a wide array of electronic properties—from insulating to highly conducting—at the ferroelectric-ferroelastic domain walls, which can greatly differ from those of the parent material.[7–13] Unlike the interfaces grown into multilayer structures that are fixed, domain walls can be created, moved, and erased by an electric field. This makes ferroelastic structures attractive for novel applications in reconfigurable electronics. Additionally, ferroelastic switching and the generation of user-defined ferroelastic-ferroelectric structures by an electric field[5,14] can provide new methodologies for (nano-)electromechanics and piezoelectric devices.[15,16] On the other hand, the electrical switching of ferroelastic structures in epitaxial films may be impeded by elastic constrains imposed by the substrate[17–21] or their elastic pinning to defects,[22] making the ferroelastic domain walls less mobile than their exclusively ferroelectric or magnetic counterparts. It is thus essential to not only engineer new ferroelastic structures, but also to assess the feasibility of the electric-field control of these structures and their stability over time.

Here we focus on the model ferroelectric $PbTiO_3$. This compound offers a rich epitaxial-strain-dependent domain phase diagram at room temperature[5,23–25] that allows a multitude of ferroelectric-ferroelastic structures. Significant progress in the electrical switching of ferroelastic domain walls between *a*- and *c*-domains—tetragonal domains with polarization parallel to the substrate-film interface and along the out-of-plane direction, respectively—has been reported, either in $PbTiO_3$ thin films or related $Pb(Zr,Ti)O_3$ films.[26–31] Electrical reconfigurability has varied considerably, ranging from a very little[29] to significant annihilation of *a*-domains

(domains with *a*-axis oriented perpendicular to the plane of the $PbTiO_3$ film).[27] To enhanced the mobility of ferroelastic domain walls, composition gradients have been employed.[30] Another approach recently applied to epitaxial films involves the possibility of modifying superdomains—ferroelastic structures comprised of an agglomerated bundle of ferroelectric domains arranged in a particular pattern[32,33]—by applying an electric field.[5] Examples of superdomains are bundles of 90° stripe domains.[32,33]

A complete picture of the ferroelastic switching in $PbTiO_3$ is lacking, especially understanding the interplay between epitaxial strain, thickness, and electric field. In this work, we systematically investigate the thickness dependence and the electrical switching of a wide variety of strained-engineered ferroelastic structures in epitaxial films of this compound. $PbTiO_3$ films, ranging from 20 to 75 nm in thickness, are grown by reactive molecular-beam epitaxy (MBE) onto (110)-oriented rare-earth (RE) scandate single-crystal substrates, where RE = Dy, Tb, Gd, and Sm. We show that the domain configuration can be effectively tuned by altering strain and film thickness simultaneously, which opens the possibility of designing, at will, different ferroelectric-ferroelastic configurations using these two variables. We find that applying an electric field can heavily disrupt the domain ground state found at a particular thickness and strain: the as-grown ferroelastic structures are all highly reconfigurable. We develop an understanding of the mechanisms underlying the ferroelastic-ferroelectric switching, the electrical rearrangement and ordering of ferroelastic structures, and in particular the stability of the electrically written domain and superdomain patterns over time. Our findings pave the way for the design of non-volatile ferroelastic structures that can be harnessed in reconfigurable nanoscale electronic circuitry,[9] in electromechanical applications,[5,29] or even in ferroelectric-based phononic devices.[34–37]

EXPERIMENTAL SECTION

Thin film growth. $PbTiO_3$ thin films were grown by MBE in a Veeco GEN 10 system using distilled ozone as an oxidant and elemental lead and titanium as source materials. Lead is supplied from a conventional MBE effusion cell, whereas titanium is sublimed from a Ti-Ball™ (Varian Associates, Vacuum Products Division).[38] During growth lead and titanium were continuously codeposited, achieving phase-pure $PbTiO_3$ in the growing film by adsorption-control, where the desorption of the excess lead supplied is controlled automatically by thermodynamics.[39] Typical lead and titanium fluxes were $1.7x10^{14}$ and $1.5x10^{13}$ atoms/(cm^2·s), respectively. Distilled ozone, which consists of about 80% O_3 and 20% O_2, was used as the oxidant.[40] The background pressure of distilled ozone during growth and the substrate temperature were fixed to $9x10^{-6}$ Torr and 600 °C, respectively. The growing film was continuously monitored by reflection high-energy electron diffraction (RHEED) to stay within the adsorption-controlled growth window.[39] After deposition, the films were cooled down at ≈100 °C/min, in a background pressure of $5x10^{-6}$ Torr of distilled ozone. $PbTiO_3$ films were grown on (110)-oriented orthorhombic $DyScO_3$, $TbScO_3$, $GdScO_3$, and $SmScO_3$ substrates that impose biaxial strains ranging from –0.25% (compressive) to +0.71% (tensile). A 10 nm thick $SrRuO_3$ layer was grown on the aforementioned substrates by MBE immediately prior to the growth of the overlying $PbTiO_3$ without breaking vacuum. These $SrRuO_3$ bottom electrodes were grown by codepositing strontium and ruthenium in an adsorption-controlled regime[41] using a mixture of O_3 (≈10%) and O_2 (≈90%) as the oxidant species. Strontium was supplied by an effusion cell, while an electron-beam evaporator was used for ruthenium. The pressure of the oxidant mixture gas and the substrate temperature were $1x10^{-6}$ Torr and 690 °C, respectively.

Thin film characterization. $\theta/2\theta$ X-ray diffraction measurements (XRD) were performed using a four-circle diffractometer (PANalytical X'Pert PRO) with Cu $K_{\alpha 1}$ radiation and the 220 reflections of a four-bounce channel-cut germanium crystal as a monochromator. Reciprocal Space Maps were performed using a four-circle diffractometer (PANalytical Empyrean) with a PIXcel^{3D} area detector. The surface topography and the ferroelectric domain and superdomain configuration were assessed by atomic force microscopy (AFM) in contact mode and piezoresponse force microscopy (PFM) in dual ac resonance track (DART) mode, respectively, using an Asylum MFP-3D Bio (Asylum Research). The typical excitation voltage was in the range of V_{ac} = 0.7-1.5 V. PtIr conducting tips (PointProbe® Plus-Electrostatic Force Microscopy from Nanosensors) were employed, with typical resonance frequencies around 350 kHz and 630 kHz for the vertical and lateral piezoresponse, respectively. To investigate the electric-field dependence of the domain and superdomain structures, a dc bias voltage is applied by the PFM tip (acting as the top electrode) on particular areas of the sample, while simultaneously scanning the domain pattern.

RESULTS AND DISCUSSION

Revisiting the strain-dependence of ferroelastic structures. The strain dependence of the domain patterns in $PbTiO_3$ films is shown in Figure 1. Details on the growth, including the RHEED and XRD patterns, can be found in the Suppl. Info. For $PbTiO_3$ grown on $DyScO_3$ the *a*/*c* ferroelastic structure prevails, similar to what has been previously reported.[42–44] This domain pattern consists of alternating *a*-domains, where the polarization lies along the in-plane pseudocubic $[100]_{pc}$ and $[010]_{pc}$ directions of the substrate, with *c*-domains, where the polarization is oriented along the out-of-plane pseudocubic $[001]_{pc}$ direction of the substrate.

Note that pseudocubic notation is used extensively in this work and the subscript pc indicates pseudocubic indices of the orthorhombic scandate substrates. The same pattern is also observed in the films grown on $TbScO_3$ substrates, yet with a higher density of domain walls, revealing that the *a*/*c* domain architecture completely dominates the ferroelectric patterns in $PbTiO_3$ from moderate compressive strains to around 0% strain. Once the strain becomes tensile, however, the domain pattern turns into a mixture of *a*/*c* and a_1/a_2 superdomains as a result of the *a*-domains being favored. Each *a*/*c* superdomain consists of a bundle of alternating *a* and *c* domains. Each a_1/a_2 superdomain consists of a bundle of alternating a_1 and a_2 domains. The a_1 domains have polarization along the pseudocubic $[100]_{pc}$ direction of the substrate. The a_2-domains have polarization along the pseudocubic $[010]_{pc}$ direction of the substrate. The larger the tensile strain, the more the *a*-domains are favored (see Fig. S2 in Suppl. Info.) and thus, the fraction of a_1/a_2 superdomains gradually increases at the expense of the *a*/*c* superdomains, in agreement with some previous reports.[5,25,37]

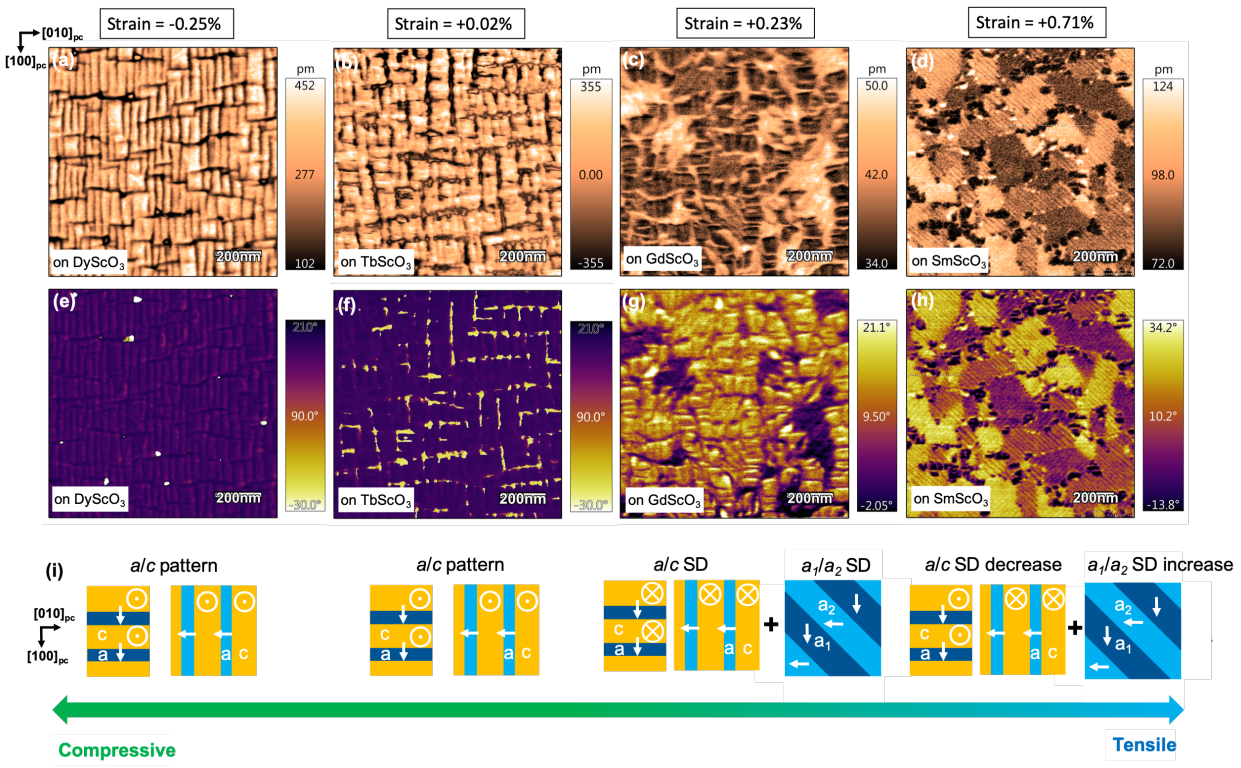

Figure 1. Vertical amplitude PFM images of **(a)** a 30 nm thick $PbTiO_3$ film on a $DyScO_3$ substrate and **(b)** a 50 nm thick $PbTiO_3$ film on a $TbScO_3$ substrate. Lateral amplitude PFM images of 20 nm thick $PbTiO_3$ films on **(c)** $GdScO_3$ and **(d)** $SmScO_3$ substrates. **(e-h)** The corresponding phase PFM images of (a-d). **(i)** Sketches indicating how the ferroelastic domain patterns in $PbTiO_3$ thin films evolve with strain.

Thickness dependence. To establish how the domain pattern evolves with film thickness, t (in the range between 20 and 75 nm), we perform PFM measurements on films of three different thicknesses at each strain value. The results are summarized in Figure 2. For moderate compressive strain (-0.25%), the type of domain architecture, *a*/*c*, remains invariant with thickness (Figure 2a-c). Yet, the *a*/*c* domain wall periodicity is found to change as the thickness increases—and, thus, the domain size enlarges—with thickness (Figure 2a-c). This is expected in any ferroic material: the energy cost of inserting a domain wall is proportional to the domain wall area and, therefore, the density of domain walls progressively diminishes with film thickness.[44–49] For the films ($t \leq 50$ nm) grown on $TbScO_3$ (nearly 0% strain), the *a*/*c* domain

configuration prevails as well, yet the *a*/*c* domain period is significantly smaller than on $DyScO_3$ for the same film thickness. This is due to the fact that on $TbScO_3$ there is an increase of the abundance of *a*-domains that must be accommodated in the same *a*/*c* architecture as on $DyScO_3$, thus, incrementing the density of *a*-domains in the *c*-matrix. For the thickest film, however, areas with low vertical piezoresponse are found between stripe-shaped regions of high vertical piezoresponse (Figure 2f), which resemble the *a*/*c* superdomains present in $PbTiO_3$ on $GdScO_3$ (Figure 2h). These low vertical piezoresponse regions correspond to a_1/a_2 superdomains as confirmed later on, yet the small size of these domains cannot be distinguished by the PFM characterization.

Very different behavior is found in films grown under tensile strain (Figure 2g-l). For $t \leq 50$ nm, the type of domain configuration remains practically the same: nearly equal populations of *a*/*c* and a_1/a_2 superdomains on $GdScO_3$ and a clear majority of a_1/a_2 superdomains on $SmScO_3$. With increasing thickness this equilibrium between *a*/*c* and a_1/a_2 populations is heavily disrupted. At $t = 75$ nm, the a_1/a_2 superdomains completely disappear in $PbTiO_3$ on $GdScO_3$ (Figure 2i) and the domain configuration becomes exclusively *a*/*c*, as though the films were grown on $DyScO_3$. On $SmScO_3$, at $t = 75$ nm, a few a_1/a_2 superdomains can still be observed (Figure 2l), reflecting the fact that at larger tensile strain values the a_1/a_2 superdomains are more favored, allowing them to survive in thicker films. Yet the domain pattern is clearly dominated by the *a*/*c* domain architecture, which is the opposite of the scenario for $t \leq 50$ nm, where a_1/a_2 superdomains prevail (Figure 2j,k). On the other hand, the size of the superdomains shows a pronounced enlargement with thickness that greatly exceeds the enlargement of the individual domains (Figure 2g-l). As a result, the density of superdomain walls decreases with increasing thickness extremely rapidly. This is similar to what happens in $BaTiO_3$ ferroelectric dots, where bands of

180° superdomains (formed by 90° domain walls) are found to increase in size as the lateral size of the dots increases.[33] Here, it is the thickness of the film that augments and affects all types of superdomains (a/c and a_1/a_2) with all kinds of superdomain walls. Superdomains thus behave as individual ferroic entities to which the same arguments used for ferromagnets,[45] ferroelectrics,[46] and ferroelastics[47] should also apply: the energy cost of adding a superdomain wall increases with film thickness. Furthermore, superdomain walls might have a significantly higher energetic cost than individual domain walls as they impose electrostatic or mechanical incompatibilities,[50] explaining their rapid decrease with increasing film thickness.

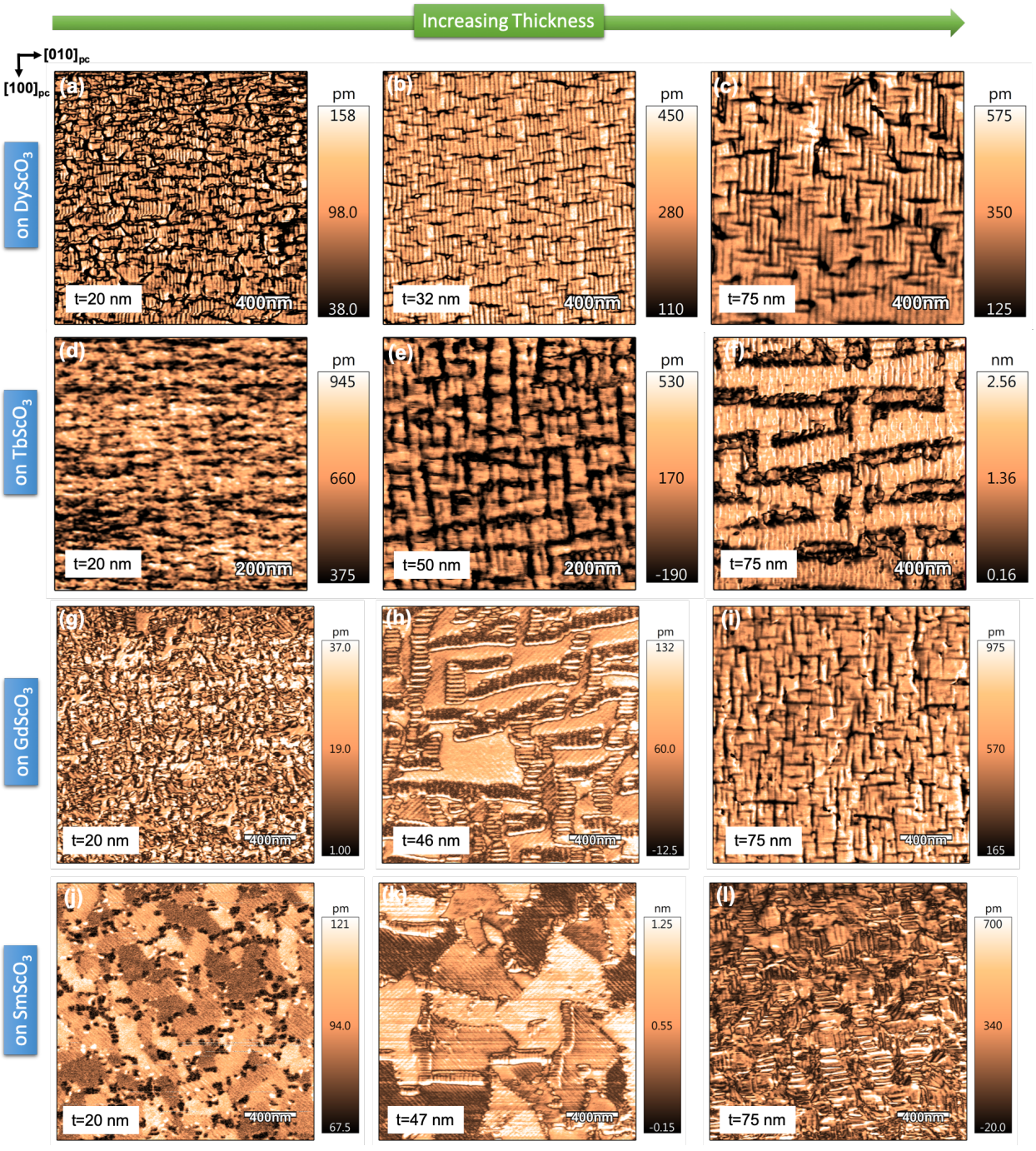

Figure 2. Vertical amplitude PFM images of $PbTiO_3$ films with different thicknesses grown on **(a-c)** $DyScO_3$ and **(d-f)** $TbScO_3$ substrates. Lateral amplitude PFM images of $PbTiO_3$ films with different thicknesses grown on **(g-i)** $GdScO_3$ and **(j-l)** $SmScO_3$ substrates. The thickness of each film is stated on each image.

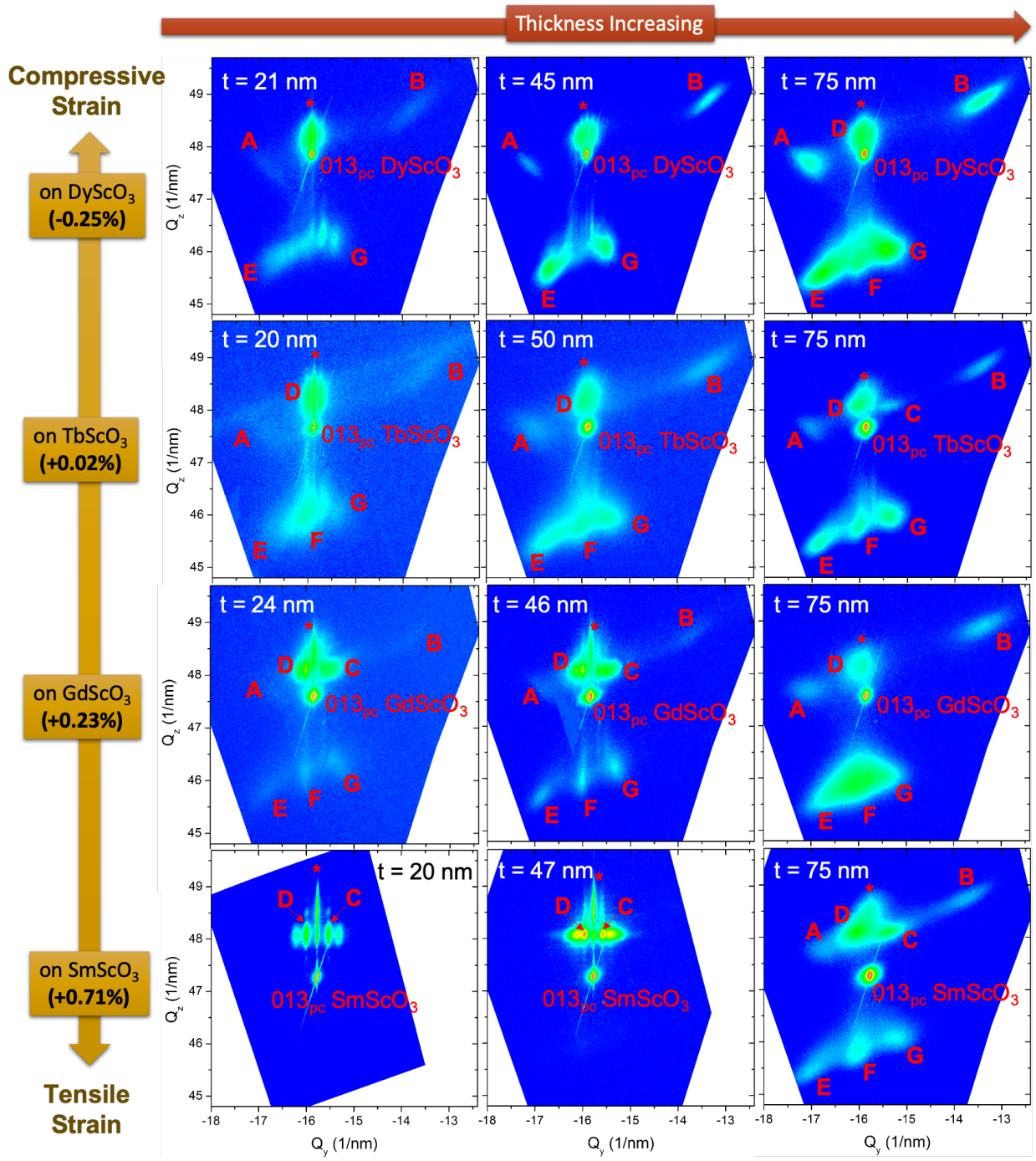

Figure 3. Thickness dependence of the Reciprocal Space Maps around the 013 reflection of $PbTiO_3$ films grown on $DyScO_3$, $TbScO_3$, $GdScO_3$, and $SmScO_3$. The thickness of each film is stated on each image. The different diffraction spots coming from the different ferroelastic domains of the $PbTiO_3$ films are labelled as A, B, C, D, E, F, and G. Figure 4 sketches these ferroelastic domains. * denotes the 013 reflection of the bottom $SrRuO_3$ electrode, which grows fully coherent onto the four different substrates.

In order to get a deeper understanding of this domain pattern evolution, Figure 3 shows the reciprocal space maps around the asymmetric 013 pseudocubic reflection of the $PbTiO_3$ films grown onto the four different substrates (four different strain values) for three different thicknesses. We have identified all the different reflection peaks coming from the $PbTiO_3$ films—labelled as A, B, C, D, E, F, and G (Figure 3)—which correspond to all the possible ferroelastic-ferroelectric domains sketched in Figure 4. It is worth noting that in order to form a coherent *a*/*c* domain wall the in-plane base of the tetragonal unit cells of the *a*- and *c*-domains are not completely parallel to the film/substrate interface when they alternate with each other in the *a*/*c* domain configuration.[37,42,51] In other words, the normal vector of the in-plane base of the unit cell of these domains is tilted with respect to the out-of-plane direction of the film (normal to the substrate interface). We refer to these domains as "tilted" in the sketch in Figure 4. Conversely, the *a*-domains forming a_1/a_2 superdomains do not tilt with respect to the out-of-plane direction,[5] that is, the in-plane base of the unit cell is parallel to the surface of the substrate. We refer to these *a*-domains as "non-tilted" in Figure 4. The 013 reflections of the a_1-domains—regardless if they are tilted or not, i.e., if they are part of the *a*/*c* or the a_1/a_2 configuration—coincide at the same position, whereas the 013 reflections of the a_2-domains split into three, one for the non-tilted domains and two for the tilted domains (Figure 4). Note that if it were around the 103 reflection, the opposite would apply (i.e., the a_1-domains would give rise to three diffraction spots and the a_2-domains would produce one spot). Similarly, the 013 reflections of the *c*-domains tilted towards the pseudocubic $[100]_{pc}$ and $[\bar{1}00]_{pc}$ directions overlap, whereas they become distinct towards the pseudocubic $[010]_{pc}$ and $[0\bar{1}0]_{pc}$ directions. Thus, in practice, the presence or absence of the diffraction spot labelled as C (corresponding to

the non-tilted a_2-domains) unequivocally means the presence or absence of a_1/a_2 superdomains, respectively.

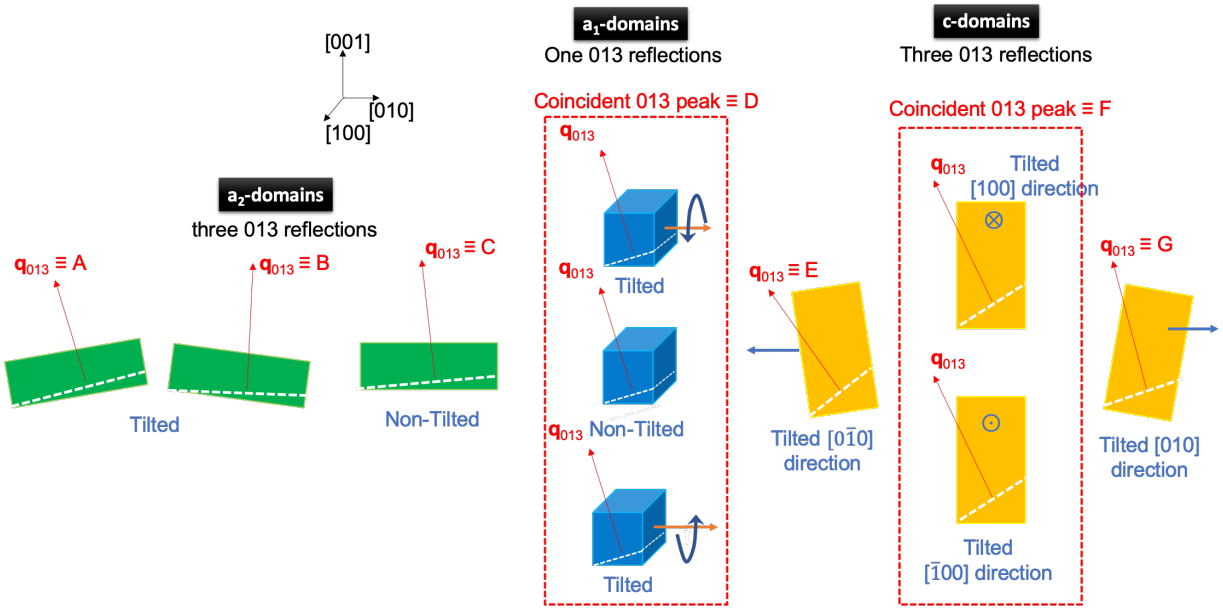

Figure 4. Sketch showing all of the possible 013 reflections for the ferroelastic domains in $PbTiO_3$ films, represented by the reciprocal space vector q_{013}. They are labelled as A, B, C, D, E, F, and G, as indicated in the reciprocal space maps in Figure 3.

In the films grown on $DyScO_3$, irrespective of thickness, only the diffraction spots corresponding to the tilted domains can be observed (Figure 3), indicating that the domain pattern remains in the *a*/*c* configuration over the whole thickness range in agreement with the PFM images (Figure 2a-c). Yet, due to the anisotropic in-plane misfit strain exerted by the $DyScO_3$ substrates (the in-plane lattice parameter along the pseudocubic $[010]_{pc}$ direction is larger than the one along the pseudocubic $[100]_{pc}$ direction), the a_2-domains are strongly favored with regard to the a_1-domains,[37] which is revealed by the absence of the D and F diffraction spots in the reciprocal space maps (Figure 3). This is also corroborated by the PFM images (Figure 2a,b) where all of the stripes of low vertical piezoresponse corresponding to the *a*-domains are aligned along the pseudocubic $[100]_{pc}$ direction (meaning they all correspond to a_2-domains[37]). Nonetheless, when

the films become thicker some a_1-domains form (yet in lower abundance than the a_2-domains) as evidenced in the PFM images (Figure 2c) and by the appearance of the F and D diffraction spots in Figure 3. For the films ($t \leq 50$ nm) grown on $TbScO_3$ the diffraction spots A, B, D, E, F, and G can be observed (Figure 3), corroborating the *a*/*c* domain pattern found in the PFM images (Figure 2) and the isotropic distribution of a_1 and a_2 domains within this *a*/*c* configuration. Note that the pseudocubic in-plane lattice parameters of (110)-oriented $TbScO_3$ are quite similar,[37] which avoids the previous anisotropic misfit strain found on (110)-oriented $DyScO_3$ substrates. For the thicker film, the C spot clearly appears, corresponding to the non-tilted a_2 domains, which can only mean the presence of a_1/a_2 superdomains, and thus confirms that the darkest regions found in the vertical PFM image in Figure 2f are certainly a_1/a_2 superdomains.

On the tensile-strain side, for the films of thickness $t \leq 50$ nm grown on $GdScO_3$, all the possible reflections sketched in Figure 4 are found in the reciprocal space maps (Figure 3). This can only mean the coexistence of *a*/*c* and a_1/a_2 superdomains in agreement with the PFM results (Figure 2). In contrast, when the tensile strain is larger (when grown on $SmScO_3$), only the C and D diffraction spots are observed in the reciprocal space maps (Figure 3) indicating that we mainly have *a*-domains forming the a_1/a_2 configuration. Nevertheless in the PFM images in Figure 2j,k some *c*-domains are observed (forming *a*/*c* superdomains), yet their abundance is too small to be detected by a macroscopic technique such as the X-ray diffraction. When the films become thicker, the diffraction pattern changes: i) the diffraction spot C disappears in the films grown on $GdScO_3$, signaling the disappearance of the a_1/a_2 superdomains as detected in the PFM images (Figure 2i); ii) additional diffraction spots (labelled as A, B, E, F, and G) appear for the films grown on $SmScO_3$ corresponding to the tilted *a*- and *c*-domains, thus indicating a greater

presence of the *a*/*c* ferroelastic configuration in the domain pattern as observed in the PFM images (Figure 2l).

This rapid thickness-dependent transition of the domain patterns in the tensile-strained $PbTiO_3$ films arises from the rapid increase in the population of *c*-domains with thickness, as proved by the θ-2θ XRD patterns (Figure 5a,b). This behavior was predicted to occur in tetragonal ferroelectric films as a mechanism to relieve epitaxial strain.[52] In practice, the thickness trend (Figure 2) is analogous to the strain trend in going from tensile to compressive strain (Figure 1), giving rise to the same domain pattern evolution: from mainly a_1/a_2 superdomains to *a*/*c* domain architectures. Thus, it is possible to design at will the type of domain architecture and the desired ratio between *a*/*c* and a_1/a_2 superdomains by selecting the appropriate strain and thickness of the $PbTiO_3$ film.

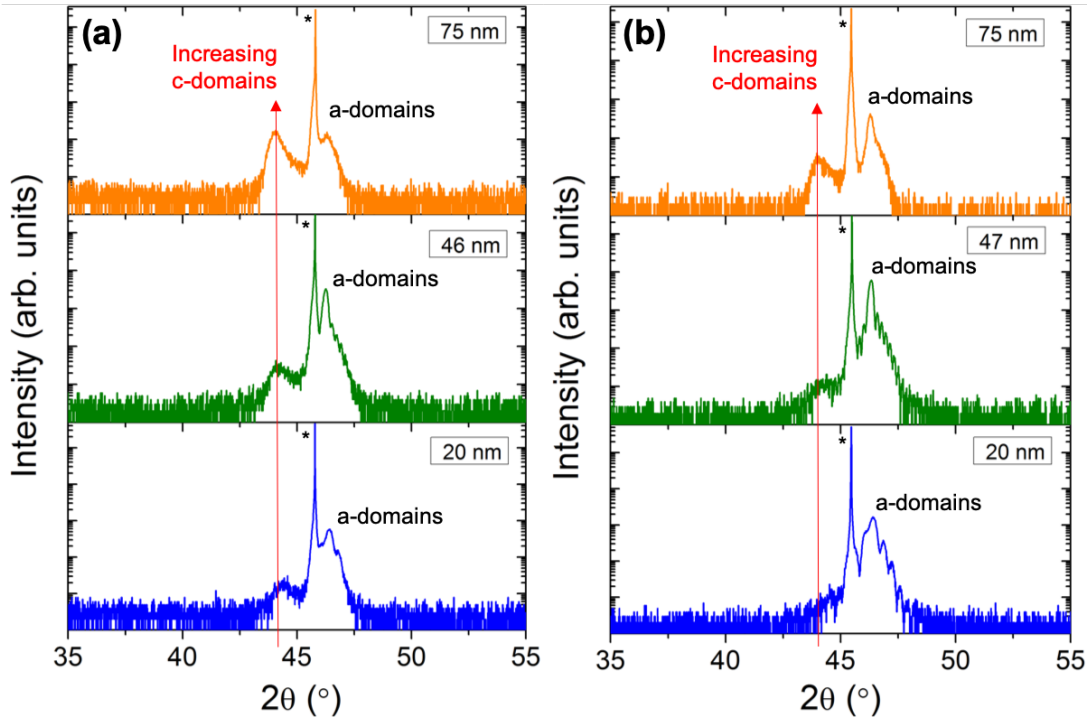

Figure 5. θ-2θ XRD scan in the vicinity of the 002 and 200 $PbTiO_3$ reflections for $PbTiO_3$ films of different thicknesses grown on **(a)** $GdScO_3$ substrates and **(b)** $SmScO_3$ substrates. The 220 peak of the substrate is indicated by an asterisk (*) in each scan.

Electric-field-control of the ferroelastic structures and their stability over time. To assess the effect of the electric field on the modification and stability of domain and superdomain patterns we applied a DC bias voltage on selected areas of the sample (i.e., along the out-of-plane direction) using a PFM tip. In particular, we investigate three types of domain architectures: *i*) *a*/*c* domain patterns ($PbTiO_3$ on $DyScO_3$), *ii*) equally populated *a*/*c* and a_1/a_2 superdomain patterns ($PbTiO_3$ on $GdScO_3$), and *iii*) mainly a_1/a_2 superdomain patterns ($PbTiO_3$ on $SmScO_3$).

Starting with *a*/*c* domain patterns ($PbTiO_3$ on $DyScO_3$), Figure 6a,b compares the domain configuration of a 75 nm thick film between the as-grown state (Figure 6a) and after applying

+3.5 V from the tip (Figure 6b) in a region marked by the dashed red rectangle. According to the phase image (Figure 6a,b bottom panels), the *c*-domains in the *a*/*c* domain pattern are switched, proving that in their as-grown state most of the polarization in these patterns is oriented toward the surface of the film (≡ upward). By applying a reverse voltage (-3.5V), the *c*-domains are switched back to the as-grown state (Figure S3 in Suppl. Info.). Note that the *a*/*c* domain structure itself is barely altered, i.e., the position and distribution of most of the *a*-domains within the *c*-matrix remain practically the same before and after applying a voltage. Similar results are found in *a*/*c* domain architectures in $PbZr_{0.3}Ti_{0.7}O_3$ films, in which very few *a*-domains were able to be annihilated.[29] The *a*/*c* domain structure thus appears to be quite robust. Yet, by applying an increased voltage (+5 V) to an as-grown region, a significant number of *a*-domains are erased so long as the electric field is applied (Figure S4 in Suppl. Info.). Therefore, reconfiguring the *a*/*c* domain architecture (which involves ferroelastic-ferroelectric switching) seems to be energetically costlier than just switching the *c*-domains within the ferroelastic structure (pure ferroelectric switching). Nonetheless, new *a*-domains appear immediately after the electric field is removed (Figure S4 in Suppl. Info.), reverting to the same density of *a*-domains as in the as-grown equilibrium state. Conversely, the pure ferroelectric switching of *c*-domains within the *a*/*c* domain architecture is extremely stable.

When the thickness is reduced (t = 32 nm), applying an out-of-plane electric field causes a noticeably larger annihilation of *a*-domains (Figure 6c,d)—compared to the thicker film—resulting in long *a*-domains, similar to what is found in $PbZr_{0.1}Ti_{0.9}O_3$ films.[27] In addition, the electrically written pattern remains after the applied voltage is removed (Figure 6d), in contrast to the thicker film (Figure 6b). Still, a few new *a*-domains gradually appear in the thinner film after several hours, whereas the poled *c*-domains remain unaltered (Figure S5 in Suppl. Info).

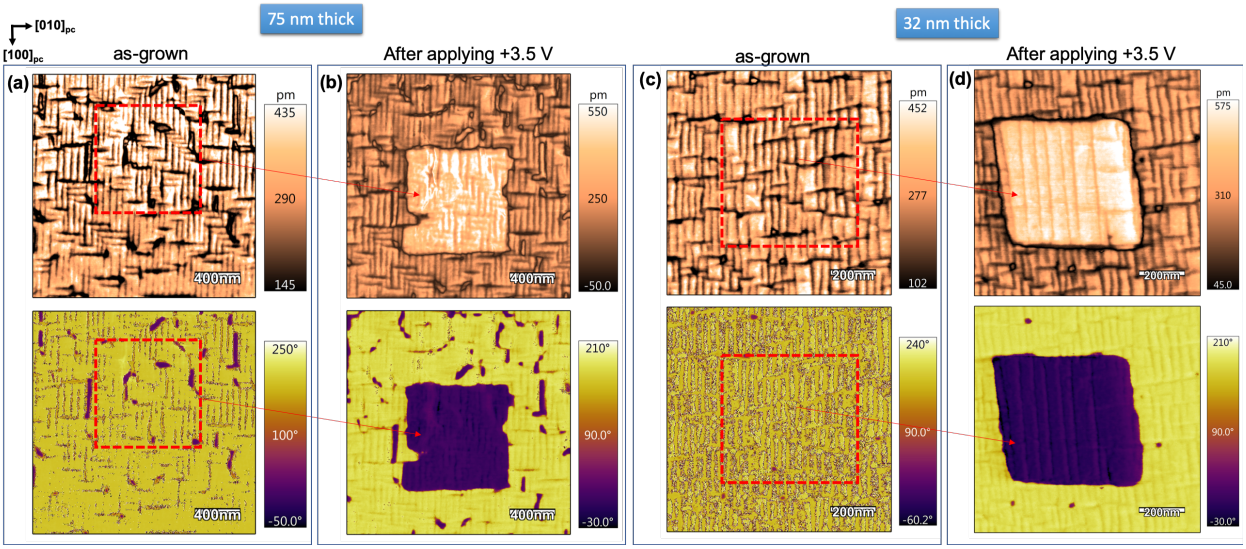

Figure 6. Vertical amplitude (top panel) and phase (bottom panel) PFM images of a 75 nm thick $PbTiO_3$ film on a $DyScO_3$ substrate **(a)** as-grown and **(b)** after applying +3.5 V to the region within the dashed red rectangle. Vertical amplitude (top panel) and phase (bottom panel) PFM images of a 32 nm thick $PbTiO_3$ film on a $DyScO_3$ substrate **(c)** as-grown and **(d)** after applying +3.5 V to the region within the dashed red rectangle.

Pure ferroelectric switching of the *c*-domains is thus seen to be robust, whereas the ferroelastic switching of the *a*/*c* patterns is not very stable. The *a*-domains form in order to relieve the accumulated elastic energy, which leads to an equilibrium ferroelastic-ferroelectric state imposed by the epitaxial strain and thickness. When altered, relaxation occurs towards the ferroelastic ground state. This altered state differs more and more from the initial state as the $PbTiO_3$ films get thicker. Relaxation is immediate in the 75 nm thick film and more progressive and incomplete in the 32 nm thick film. The depolarizing field does not depend on thickness and moreover it can be screened over time. In contrast, elastic energy is proportional to the thickness and can never be screened. Therefore, it makes sense that, as films get thicker, elastic forces dominate over electrostatic ones and thus the films revert faster to their original ferroelastic configuration. This finding is important to consider when it comes to designing functional

properties at *a*/*c* domain walls[9] or non-volatile ferroelastic switching devices based on *a*/*c* domain architectures.[29]

We now assess the scenario in which *a*/c and a_1/a_2 superdomains coexist with almost equal populations as is the case for $PbTiO_3$ (t < 50 nm) on $GdScO_3$. Figure 7a analyzes the effects of applying a positive voltage from the PFM tip. In order to reveal the a_1/a_2 superdomains, both the vertical and lateral piezoresponse of the as-grown superdomain patterns are shown. The black areas in the amplitude of the vertical PFM image (which means no vertical piezoresponse) correspond to the a_1/a_2 superdomains. We monitor the electric-field dependence and time evolution of the superdomains by just recording vertical PFM images. While applying the +5V bias voltage, the as-grown superdomain pattern turns completely into an *a*/*c* domain architecture. This is the same domain pattern found in $PbTiO_3$ on $DyScO_3$. In other words, an applied out-of-plane electric field is capable of effectively erasing and moving all of the ferroelastic domain and superdomain walls, transforming all a_1/a_2 superdomains into *a*/*c* superdomains and expanding the existing as-grown *a*/*c* superdomains. Immediately after removing the electric field, however, a few new a_1/a_2 superdomains reappear, driven by the epitaxial strain exerted by the substrate. These a_1/a_2 superdomains try to pull the system back into the as-grown equilibrium state as discussed previously. Still, the new electrically written superdomain pattern notably contains more *a*/*c* superdomains than the as-grown scenario. Interestingly, the polarization in the *c*-domains is not switched; the phase in the vertical PFM image remains unchanged (Figure 7a bottom panels) before, during, and after applying the positive voltage. Therefore, expansion of the ferroelastic-ferroelectric *a*/*c* superdomain walls occurs without ferroelectric switching of the polarization of the individual *c* domains.

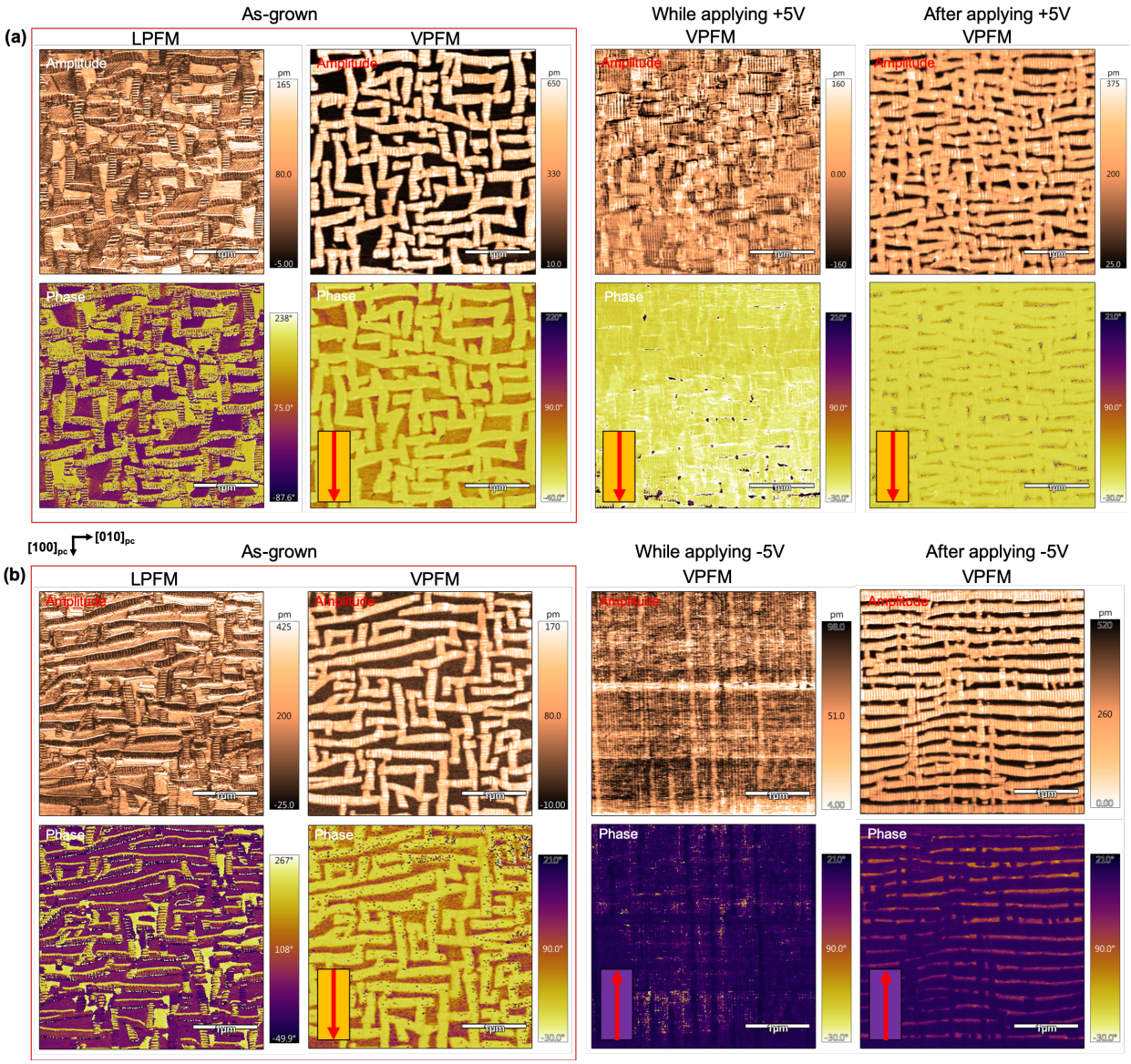

Figure 7. (a) Effects of applying a positive voltage and **(b)** a negative voltage from the PFM tip to a 46 nm thick $PbTiO_3$ film on a $GdScO_3$ substrate. Top panels and bottom panels in **(a,b)** correspond to amplitude and phase PFM images, respectively. LPFM and VPFM stand for lateral and vertical PFM.

When a negative dc bias voltage from the PFM tip is applied (Figure 7b), the change in the phase in the vertical piezoresponse indicates that the *c*-domains have been poled upward. This confirms that the *c*-domains are poled downward in the as-grown film. The whole domain pattern turns

into an *a*/*c* domain pattern while writing, erasing the a_1/a_2 superdomains like in the previous situation. Nevertheless, here the *a*- and *c*-domains are extremely ordered during writing. All of them extend in the same in-plane $[100]_{pc}$ direction (the vertical direction in the PFM image) for a few microns (Figure 7b), which does not occur when the *c*-domains are not switched (Figure 7a). When the applied electric field is removed, some new a_1/a_2 superdomains reappear in the same way as when a positive voltage is utilized, signaling the partial relaxation of the written *a*/*c* structure. Still, as a result of the *a*/*c* order during the writing, the resulting pattern is no longer a maze-distributed *a*/*c* superdomains as previously seen (Figure 7a). It is transformed into a substantially ordered pattern with *a*/*c* superdomain stripes along the $[010]_{pc}$ direction (Figure 7b).

Close inspection of Figure 7a (third column) reveals that when no ferroelectric switching of the as-grown *c*-domains occurs, the existing as-grown *a*/*c* superdomains are expanded instead of them being reconfigured completely. The original distribution of superdomains is preserved, producing the maze-shaped morphology. Conversely, when a negative voltage is applied and the polarization of the as-grown *c*-domains is reversed (Figure 7b), the whole superdomain pattern is reconfigured, completely erasing both the as-grown *a*/*c* and a_1/a_2 superdomains to create a totally new ferroelastic structure. It thus turns out that the ferroelectric switching of the *c*-domains in the *a*/*c* superdomains is key to completely restructuring them and explains the significantly different morphology achieved (maze-distribution vs ordered stripes) from the application of a positive vs a negative voltage to the PFM tip. This finding is crucial when it comes to designing nanostructured patterns in specific nanostructured superdomains. The preferential orientation of the *a*/*c* stripes along the $[010]_{pc}$ direction is caused by dynamic writing as the PFM tip is scanning along this direction, creating the long *a* and *c* domains along the $[100]_{pc}$ direction.

Hence, it is even possible to change the direction of the nanostructured *a*/*c* superdomains by 90° just by changing the scan angle of the PFM tip.

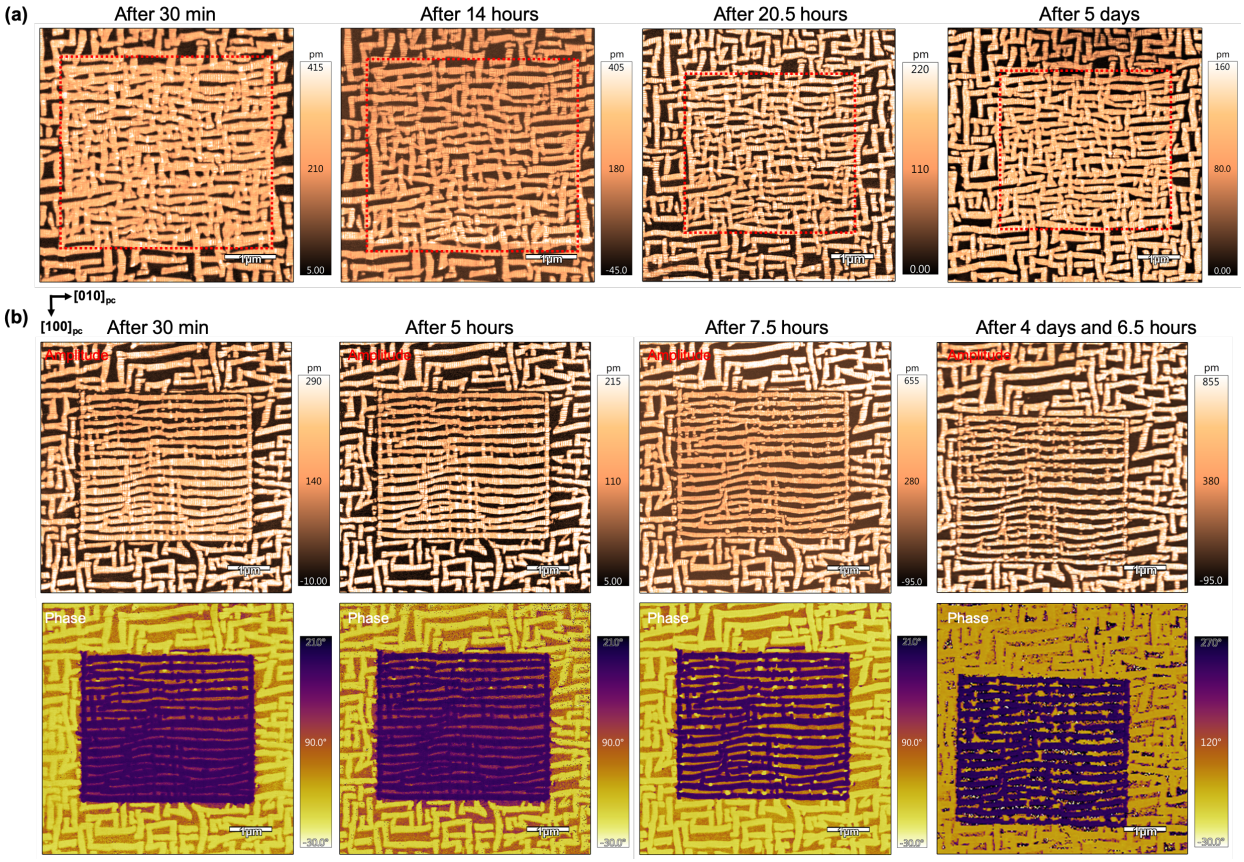

Figure 8. (a) Vertical amplitude PFM images showing the time evolution of the written maze-shaped *a*/*c* superdomains in a 46 nm thick $PbTiO_3$ film on a $GdScO_3$ substrate after the removal of a +5 V tip bias from the region within the dashed red rectangle. **(b)** Vertical amplitude (top panels) and phase (bottom panels) PFM images showing the time evolution of the written stripe-shaped ordered *a*/*c* superdomains in a 46 nm thick $PbTiO_3$ film on a $GdScO_3$ substrate after the removal of a –5 V tip bias from the region within the dashed red rectangle.

The stability over time of the written *a*/*c* superdomains (both maze-distributed and ordered stripes) is shown in Figure 8. The electric field was applied to the area delimited by the dashed red rectangle. As is evident, the electrically written ferroelastic structures are rather robust. They

last for at least several days in this form after the applied voltage is removed. An expansion of the a_1/a_2 superdomains is evident in the initial hours, which gradually compresses the a/c superdomains. This shows that parts of the a/c superdomains relax into a_1/a_2 superdomains by moving the superdomain walls, making the former smaller, instead of completely turning the whole superdomain into a_1/a_2. The latter would appear as a change in the maze-shape or stripe-shape superdomain pattern. The expansion of the a_1/a_2 domains slows down over time and the final stable written structure contains a higher density of a/c superdomains than the as-grown one, as we quantify in the next Section. Hence, it is possible to stabilize long-lasting metastable superdomain configurations in $PbTiO_3$ on $GdScO_3$. On the other hand, the upward-poled c-domains of the stripe-shape pattern are mainly maintained; a few c-domains flip their polarization to the as-grown state after several days (Figure 8b bottom panel).

For thinner films (~20 nm) grown on $GdScO_3$ the domain pattern is fully transformed by applying a vertical voltage into an a/c domain architecture. All of the a_1/a_2 superdomains are erased as is shown in Figure S6 of the Suppl. Info. It is as if the $PbTiO_3$ were grown on $DyScO_3$. Moreover, no relaxation of the pattern is seen with time, further establishing the strong stability of the electrically switched ferroelastic structures in $PbTiO_3$ films grown on $GdScO_3$.

The electric-field dependence of a domain architecture dominated by a_1/a_2 superdomains ($PbTiO_3$ on $SmScO_3$) is shown in Figure 9. During writing the whole domain pattern transforms into an a/c domain architecture, as also occurs when a voltage is applied to $PbTiO_3$ on $GdScO_3$, even though in this $PbTiO_3$ on $SmScO_3$ case we start from a mainly a_1/a_2 superdomain structure. Thus, even if the epitaxial strain determines a strong presence of a_1/a_2 domains, the application of a vertical voltage is able to turn all of them into a/c patterns. This demonstrates the high electrically malleability of the ferroelastic structures in $PbTiO_3$ when different types of

superdomains coexist. The electrically written *a*/*c* superdomains are, however, rather short lived once the electric field is removed. In contrast to the relaxation that occurs for $PbTiO_3$ on $GdScO_3$, here all of the *a*/*c* superdomains revert to a_1/a_2 superdomains, progressively disappearing over time as shown in Figure 9. Similar rapid reversion to the as-grown equilibrium a_1/a_2 domain pattern is also found for thinner $PbTiO_3$ on $SmScO_3$ films (see Figure S7 of the Suppl. Info.). Thus, the large tensile strain imposed by the $SmScO_3$ substrate (+0.71%) prevents the written *a*/*c* superdomains from lasting, precluding the stabilization of nanoscale ferroelastic structures in this case. Nonetheless, it is worth noting that some residual *a*/*c* superdomains after switching look like droplets, similar to the bubble domains found in 180-degree domain configurations.[53] These ferroelastic "bubble superdomains" are a rare feature as these kinds of structures are generally absent in ferroelastic domain configurations.

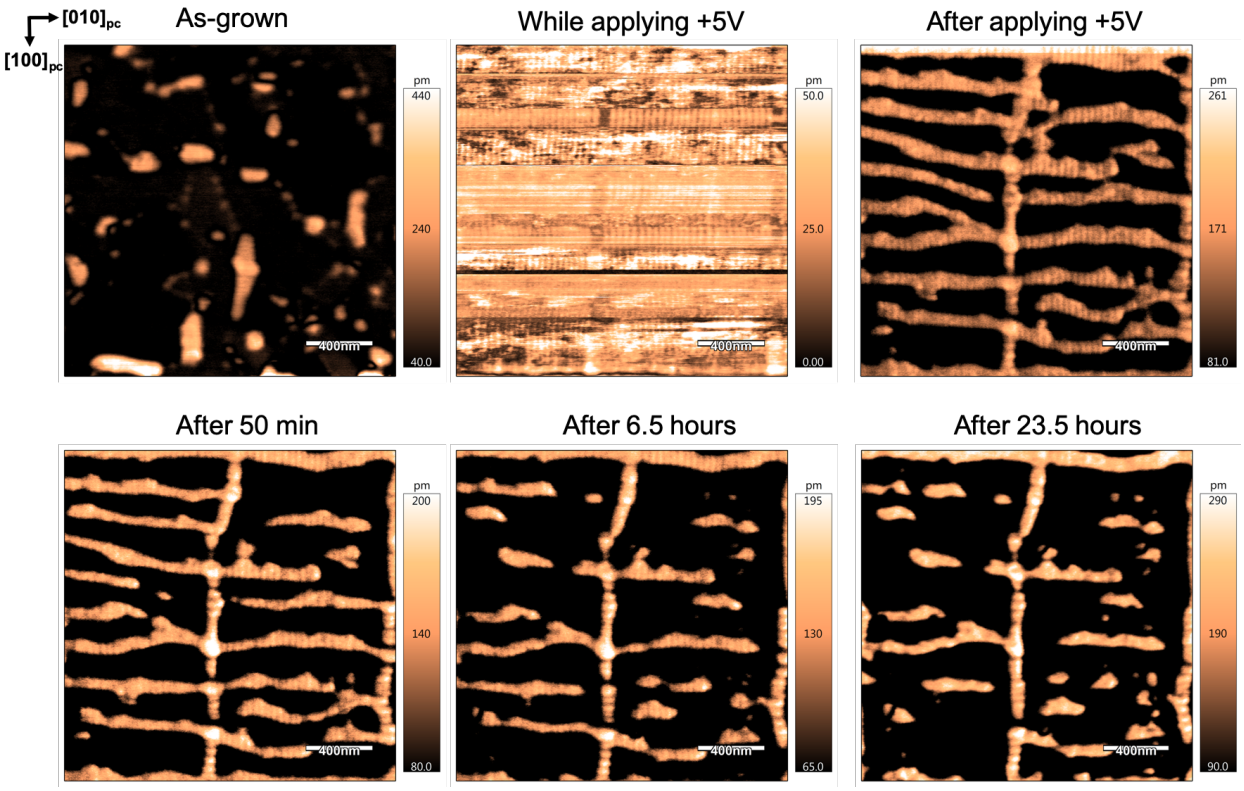

Figure 9. Vertical amplitude PFM images showing the as-grown pattern of a 47 nm thick $PbTiO_3$ film grown on a $SmScO_3$ substrate, how it changes when +5 V is applied, and the time evolution of the written *a*/*c* superdomains after the voltage is removed from the PFM tip.

Note the lack of uniformity in the orientation of the polarization of the *c* domains in the as-grown *a*/*c* superdomains in $PbTiO_3$ on $SmScO_3$ (see Figure S8 in Suppl. Info.). Within a particular as-grown *a*/*c* superdomain all of the *c*-domains possess the same polarization direction, either up or down. This implies a nearly equal distribution of up/down *a*/*c* superdomains and contrasts with the previous cases where a unique out-of-plane polarization was observed over the whole sample. This may explain the less ordered *a*/*c* stripes that can be written on $SmScO_3$. The lack of a unique out-of-plane polarization direction means that regardless of whether a positive or negative dc bias voltage is applied to the as-grown *a*/*c* superdomains, the out-of-plane

polarization of many of the superdomains will point in the same direction as the external electric field, resulting in a mix between maze- and stripe-shaped *a/c* superdomains.

Time relaxation of the electrically written *a/c* superdomains. We quantify the time evolution of the relaxation of the written *a/c* superdomains into a_1/a_2 superdomains, both when they become narrower (on $GdScO_3$) and when they disappear (on $SmScO_3$). To do so, we have computed the amplitude of the vertical PFM images of ~50 nm thick films on both substrates to account for the quantity of a_1/a_2 and *a*/*c* superdomains present at each time. The quantity of a_1/a_2 and *a*/*c* superdomains are shown in black and orange in Figure S9 of the Supplemental Info. Figure 10 shows the time dependence of the areal percentage occupied by *a*/*c* superdomains in the PFM image, starting at time = 0 when the voltage is applied (which corresponds to 100% of the total area). On both $GdScO_3$ and $SmScO_3$ substrates a rapid decrease in *a*/*c* superdomains occurs after the applied voltage is removed, which slows down over time. The relaxation of domains in other ferroic materials tends to follow either an exponential or a power law decay,[3] which suggests that our superdomain structures could display similar trends. The exponential decay was found to fit our data better. The solid orange line in Figure 10 depicts the experimental data fit to the exponential function $y = A_0\exp(-t'/\tau_0) + y_0$, where y is the percentage of *a*/*c* superdomains in the pattern, A_0 is a proportional constant which accounts for the initial fraction of *a*/*c* superdomains induced by the electric field (at $t' = 0$), t' is time, τ_0 is the relaxation time, and y_0 is the residual presence of *a*/*c* superdomains for $t' \rightarrow \infty$. The A_0 and τ_0 values depend on the elastic energy cost of the superdomains, which in turn depends on thickness and mismatch strain. The larger either of these quantities is, the faster the relaxation will proceed. The fit matches the data reasonably well, better on $GdScO_3$ than on $SmScO_3$. This may be due to the superdomains disappearing completely on $SmScO_3$ instead of the more gradual shrinking that

occurs on $GdScO_3$. The relaxation time—accounting for how quickly the relaxation process takes place—is much larger (200% larger) on $GdScO_3$ ($\tau_0 \sim 18$ minutes) than on $SmScO_3$ ($\tau_0 \sim 9$ minutes). This reflects the significantly faster conversion of written *a*/*c* superdomains into a_1/a_2 superdomains with increasing tensile strain (as qualitatively revealed in Figures 8 and 9). y_0 is found to be slightly larger than the areal occupation of *a*/*c* superdomains in the as-grown films for both scenarios. This implies that the relaxation process is incomplete on both substrates and that the final domain configuration after applying the out-of-plane voltage is enriched in *a*/*c* superdomains compared to the as-grown scenario.

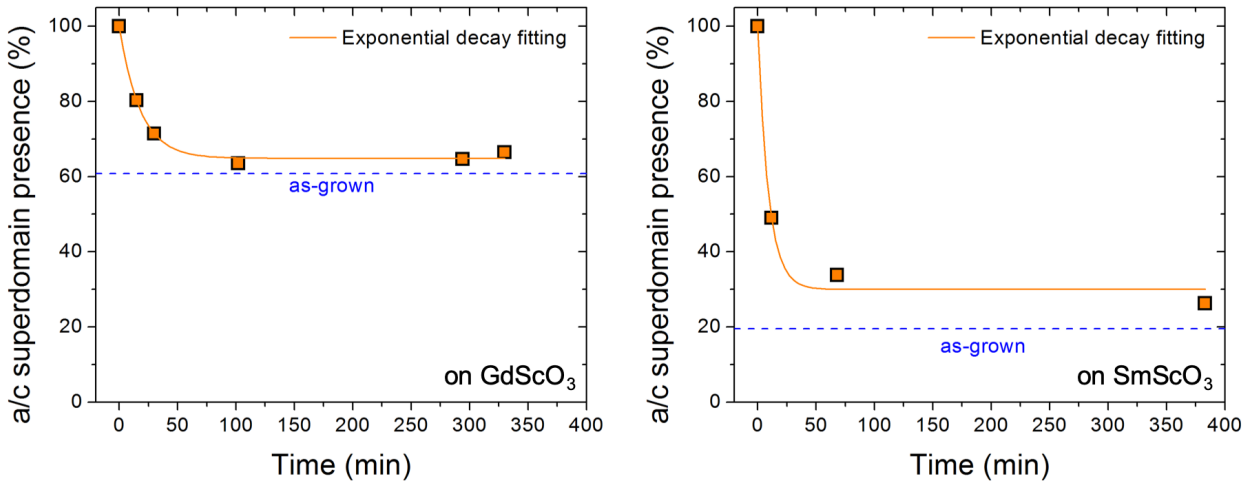

Figure 10. Time evolution of the areal percentage of *a*/*c* superdomains after the removal of the electric field at time zero. The left panel corresponds to a 46 nm thick $PbTiO_3$ film grown on $GdScO_3$ and the right panel corresponds to a 47 nm thick $PbTiO_3$ film grown on $SmScO_3$. The solid orange line corresponds to an exponential decay model (see text for the expression) and the dashed blue line represents the areal percentage of *a*/*c* superdomains in the films before applying the electric field, i.e., in their as-grown state.

CONCLUSIONS

In summary, we have systematically investigated the evolution of ferroelastic structures in $PbTiO_3$ films as a function of epitaxial strain, film thickness, and voltage applied by a PFM tip. The kind of domain architecture does not change with thickness for exclusively *a*/*c* domain patterns, but it does when the domain patterns contain a mixture of *a*/*c* and a_1/a_2 superdomains. Specifically, the presence of *c*-domains significantly increases with film thickness, promoting the increase of *a*/*c* superdomains at the expense of a_1/a_2 superdomains. We find that the balance between *a*/*c* and a_1/a_2 superdomains can be tipped, not only by strain, but also by thickness, providing an extra degree of freedom to engineer ferroelastic structures. We also show that the ferroelastic structures in $PbTiO_3$ are quite malleable when an electric field is applied. The *a*/*c* domain architectures can be completely reconfigured by annihilating most of the *a*-domains. The stability of the new pattern is, however, short-lived, especially for thicker films. When *a*/*c* and a_1/a_2 superdomains coexist, the out-of-plane electric field turns all a_1/a_2 superdomains into *a*/*c* superdomains. The ferroelectric switching of *c*-domains is found to be essential to imparting designed *a*/*c* superdomain morphologies. Larger tensile strains destabilize the written *a*/*c* superdomains. At a biaxial strain of 0.71% ($PbTiO_3$ on $SmScO_3$) these quickly decay—relaxing to a_1/a_2 superdomains—when the electric field is removed. Only for low tensile strains (e.g., $PbTiO_3$ on $GdScO_3$) are electrically created *a*/*c* superdomains stable for days. Our findings demonstrate the feasibility of tailoring stable ferroelastic structures in $PbTiO_3$ films that are relevant to non-volatile electromechanical applications or reconfigurable nanoscale electrical properties.

ASSOCIATED CONTENT

Supporting Information. Additional information is provided on the epitaxial growth and structural characterization of the $PbTiO_3$ thin films, piezoresponse force microscopy experiments, and computation of the relaxation of the electrically written *a*/*c* superdomains.

AUTHOR INFORMATION

Corresponding Author

*E-mail: eric.langenberg.perez@gmail.com and schlom@cornell.edu

Notes

The authors declare no competing financial interest.

ACKNOWLEDGMENT

E.L. acknowledges funding received from the European Union's Horizon 2020 research and innovation program through the Marie Skłodowska-Curie Actions: Individual Fellowship-Global Fellowship (Ref. MSCA-IF-GF-708129). The work at Cornell University was supported by the Army Research Office under grant W911NF-16-1-0315. H.P. acknowledges support from the National Science Foundation [Platform for the Accelerated Realization, Analysis, and Discovery of Interface Materials (PARADIM)] under Cooperative Agreement No. DMR-1539918.

REFERENCES

(1) Salje, E. K. H. Ferroelastic Materials. *Annu. Rev. Mater. Res.* **2012**, *42*, 265–283.
(2) Sharma, P.; McQuaid, R. G. P.; McGilly, L. J.; Gregg, J. M.; Gruverman, A. Nanoscale Dynamics of Superdomain Boundaries in Single-Crystal $BaTiO_3$ Lamellae. *Adv. Mater.* **2013**, *42*, 265–283.
(3) Scott, J. F.; Hershkovitz, A.; Ivry, Y.; Lu, H.; Gruverman, A.; Gregg, J. M. Superdomain Dynamics in Ferroelectric-Ferroelastic Films: Switching, Jamming, and Relaxation. *Appl. Phys. Rev.* **2017**, *4*, 041104.

(4) Braun, D.; Schmidbauer, M.; Hanke, M.; Kwasniewski, A.; Schwarzkopf, J. Tunable Ferroelectric Domain Wall Alignment in Strained Monoclinic $K_xNa_{1-x}NbO_3$ Epitaxial Films. *Appl. Phys. Lett.* **2017**, *110*, 232903.
(5) Damodaran, A. R.; Pandya, S.; Agar, J. C.; Cao, Y.; Vasudevan, R. K.; Xu, R.; Saremi, S.; Li, Q.; Kim, J.; McCarter, M. R.; Dedon, L. R.; Angsten, T.; Balke, N.; Jesse, S.; Asta, M. Kalinin, S. V.; Martin, L. W. Three-State Ferroelastic Switching and Large Electromechanical Responses in $PbTiO_3$ Thin Films. *Adv. Mater.* **2017**, 1702069.
(6) Alsubaie, A.; Sharma, P.; Lee, J. H.; Kim, J. Y.; Yang, C. H.; Seidel, J. Uniaxial Strain-Controlled Ferroelastic Domain Evolution in $BiFeO_3$. *ACS Appl. Mater. Interfaces* **2018**, *10*, 11768–11775.
(7) Seidel, J.; Martin, L. W.; He, Q.; Zhan, Q.; Chu, Y. H.; Rother, A.; Hawkridge, M. E.; Maksymovych, P.; Yu, P.; Gajek, M.; Balke, N.; Kalinin, S. V.; Gemming, S.; Wang, F.; Catalan, G.; Scott, J. F.; Spaldin, N. A.; Orenstein, J.; Ramesh, R. Conduction at Domain Walls in Oxide Multiferroics. *Nat. Mater.* **2009**, *8*, 229–234.
(8) Sluka, T.; Tagantsev, A. K.; Bednyakov, P.; Setter, N. Free-Electron Gas at Charged Domain Walls in Insulating $BaTiO_3$. *Nat. Commun.* **2013**, *4*, 1808.
(9) Stolichnov, I.; Feigl, L.; McGilly, L. J.; Sluka, T.; Wei, X. K.; Colla, E.; Crassous, A.; Shapovalov, K.; Yudin, P.; Tagantsev, A. K.; Setter, N. Bent Ferroelectric Domain Walls as Reconfigurable Metallic-Like Channels. *Nano Lett.* **2015**, *15*, 8049–8055.
(10) Becher, C.; Maurel, L.; Aschauer, U.; Lilienblum, M.; Magén, C.; Meier, D.; Langenberg, E.; Trassin, M.; Blasco, J.; Krug, I. P.; Algarabel, P. A.; Spaldin, N. A.; Pardo, J. A.; Fiebig, M. Strain-Induced Coupling of Electrical Polarization and Structural Defects in $SrMnO_3$ Films. *Nat. Nanotechnol.* **2015**, *10*, 661–666.
(11) Li, L.; Britson, J.; Jokisaari, J. R.; Zhang, Y.; Adamo, C.; Melville, A.; Schlom, D. G.; Chen, L. Q.; Pan, X. Giant Resistive Switching via Control of Ferroelectric Charged Domain Walls. *Adv. Mater.* **2016**, *28*, 6574–6580.
(12) Campbell, M. P.; McConville, J. P. V.; McQuaid, R. G. P.; Prabhakaran, D.; Kumar, A.; Gregg, J. M. Hall Effect in Charged Conducting Ferroelectric Domain Walls. *Nat. Commun.* **2016**, *7*, 13764.
(13) Mundy, J. A.; Schaab, J.; Kumagai, Y.; Cano, A.; Stengel, M.; Krug, I. P.; Gottlob, D. M.; Doğanay, H.; Holtz, M. E.; Held, R.; Yan, Z.; Bourret, E.; Schneider, C. M.; Schlom, D. G.; Muller, D. A.; Ramesh, R.; Spaldin, N. A.; Meier, D. Functional Electronic Inversion Layers at Ferroelectric Domain Walls. *Nat. Mater.* **2017**, *16*, 622–627.
(14) Agar, J. C.; Cao, Y.; Naul, B.; Pandya, S.; van der Walt, S.; Luo, A. I.; Maher, J. T.; Balke, N.; Jesse, S.; Kalinin, S. V.; Vasudevan, R. K.; Martin, L. W. Machine Detection of Enhanced Electromechanical Energy Conversion in $PbZr_{0.2}Ti_{0.8}O_3$ Thin Films. *Adv. Mater.* **2018**, 1800701.
(15) Loh, O. Y.; Espinosa, H. D. Nanoelectromechanical Contact Switches. *Nat. Nanotechnol.* **2012**, *7*, 283–295.
(16) Solomon, P. M.; Bryce, B. A.; Kuroda, M. A.; Keech, R.; Shetty, S.; Shaw, T. M.; Copel, M.; Hung, L. W.; Schrott, A. G.; Armstrong, C.; Gordon, M. S.; Reuter, K. B.; Theis, T. N.; Haensch, W.; Rossnagel, S. M; Miyazoe, H.; Elmegreen, B. G.; Liu, X.-H.; Trolier-McKinstry, S.; Martyna, G. J.; Newns, D. M. Pathway to the Piezoelectronic Transduction Logic Device. *Nano Lett.* **2015**, *15*, 2391–2395.
(17) Nagarajan, V.; Roytburd, A.; Stanishevsky, A.; Prasertchoung, S.; Zhao, T.; Chen, L.; Melngailis, J.; Auciello, O.; Ramesh, R. Dynamics of Ferroelastic Domains in

Ferroelectric Thin Films. *Nat. Mater.* **2003**, *2*, 43–47.
(18) Baek, S. H.; Jang, H. W.; Folkman, C. M.; Li, Y. L.; Winchester, B.; Zhang, J. X.; He, Q.; Chu, Y. H.; Nelson, C. T.; Rzchowski, M. S.; Pan, X. Q.; Ramesh, R.; Chen, L. Q.; Eom, C. B. Ferroelastic Switching for Nanoscale Non-Volatile Magnetoelectric Devices. *Nat. Mater.* **2010**, *9*, 309–314.
(19) Griggio, F.; Jesse, S.; Kumar, A.; Ovchinnikov, O.; Kim, H.; Jackson, T. N.; Damjanovic, D.; Kalinin, S. V.; Trolier-Mckinstry, S. Substrate Clamping Effects on Irreversible Domain Wall Dynamics in Lead Zirconate Titanate Thin Films. *Phys. Rev. Lett.* **2012**, *108*, 157604.
(20) Wang, C.; Ke, X.; Wang, J.; Liang, R.; Luo, Z.; Tian, Y.; Yi, D.; Zhang, Q.; Wang, J.; Han, X. F.; van Tendeloo, G.; Chen, L. Q.; Nan, C.-W.; Ramesh, R.; Zhang, J. Ferroelastic Switching in a Layered-Perovskite Thin Film. *Nat. Commun.* **2016**, *7*, 10636.
(21) Ullah, R.; Ke, X.; Malik, I. A.; Gu, Z.; Wang, C.; Ahmad, M.; Yang, Y.; Zhang, W.; An, X.; Wang, X.; Zhang, J. Controllable Ferroelastic Switching in Epitaxial Self-Assembled Aurivillius Nanobricks. *ACS Appl. Mater. Interfaces* **2019**, *11*, 7296–7302.
(22) Su, D.; Meng, Q.; Vaz, C. A. F.; Han, M. G.; Segal, Y.; Walker, F. J.; Sawicki, M.; Broadbridge, C.; Ahn, C. H. Origin of 90° Domain Wall Pinning in $Pb(Zr_{0.2}Ti_{0.8})O_3$ Heteroepitaxial Thin Films. *Appl. Phys. Lett.* **2011**, *99*, 102902.
(23) Waser, R.; Pertsev, N. A.; Koukhar, V. G. Thermodynamic Theory of Epitaxial Ferroelectric Thin Films with Dense Domain Structures. *Phys. Rev. B - Condens. Matter Mater. Phys.* **2001**, *64*, 214103.
(24) Li, Y. L.; Hu, S. Y.; Liu, Z. K.; Chen, L. Q. Effect of Substrate Constraint on the Stability and Evolution of Ferroelectric Domain Structures in Thin Films. *Acta Mater.* **2002**, *50*, 395–411.
(25) Sheng, G.; Zhang, J. X.; Li, Y. L.; Choudhury, S.; Jia, Q. X.; Liu, Z. K.; Chen, L. Q. Domain Stability of $PbTiO_3$ Thin Films under Anisotropic Misfit Strains: Phase-Field Simulations. *J. Appl. Phys.* **2008**, *104*, 054105.
(26) Ivry, Y.; Wang, N.; Chu, D.; Durkan, C. 90° Domain Dynamics and Relaxation in Thin Ferroelectric/Ferroelastic Films. *Phys. Rev. B* **2010**, *81*, 174118.
(27) Feigl, L.; McGilly, L. J.; Sandu, C. S.; Setter, N. Compliant Ferroelastic Domains in Epitaxial $Pb(Zr,Ti)O_3$ Thin Films. *Appl. Phys. Lett.* **2014**, *104*, 172904.
(28) Gao, P.; Britson, J.; Nelson, C. T.; Jokisaari, J. R.; Duan, C.; Trassin, M.; Baek, S. H.; Guo, H.; Li, L.; Wang, Y.; Chu, Y.-H.; Minor, A. M.; Eom, C. B.; Ramesh, R.; Chen, L. Q.; Pan, X. Ferroelastic Domain Switching Dynamics under Electrical and Mechanical Excitations. *Nat. Commun.* **2014**, *5*, 3801.
(29) Khan, A. I.; Marti, X.; Serrao, C.; Ramesh, R.; Salahuddin, S. Voltage-Controlled Ferroelastic Switching in $Pb(Zr_{0.2}Ti_{0.8})O_3$ Thin Films. *Nano Lett.* **2015**, *15*, 2229–2234.
(30) Agar, J. C.; Damodaran, A. R.; Okatan, M. B.; Kacher, J.; Gammer, C.; Vasudevan, R. K.; Pandya, S.; Dedon, L. R.; Mangalam, R. V. K.; Velarde, G. A.; Jesse, S.; Balke, N.; Minor, A. M.; Kalinin, S. V.; Martin, L. W. Highly Mobile Ferroelastic Domain Walls in Compositionally Graded Ferroelectric Thin Films. *Nat. Mater.* **2016**, *15*, 549–557.
(31) Li, M.; Wang, B.; Liu, H. J.; Huang, Y. L.; Zhang, J.; Ma, X.; Liu, K.; Yu, D.; Chu, Y. H.; Chen, L. Q.; Gao, P. Direct Observation of Weakened Interface Clamping Effect Enabled Ferroelastic Domain Switching. *Acta Mater.* **2019**, *171*, 184–189.
(32) McGilly, L. J.; Schilling, A.; Gregg, J. M. Domain Bundle Boundaries in Single Crystal $BaTiO_3$ Lamellae: Searching for Naturally Forming Dipole Flux-Closure/Quadrupole

Chains. *Nano Lett.* **2010**, *10*, 4200–4205.
(33) Mcgilly, L. J.; Gregg, J. M. Scaling of Superdomain Bands in Ferroelectric Dots. *Appl. Phys. Lett.* **2011**, *98*, 132902.
(34) Ihlefeld, J. F.; Foley, B. M.; Scrymgeour, D. A.; Michael, J. R.; McKenzie, B. B.; Medlin, D. L.; Wallace, M.; Trolier-Mckinstry, S.; Hopkins, P. E. Room-Temperature Voltage Tunable Phonon Thermal Conductivity via Reconfigurable Interfaces in Ferroelectric Thin Films. *Nano Lett.* **2015**, *15*, 1791–1795.
(35) Seijas-Bellido, J. A.; Escorihuela-Sayalero, C.; Royo, M.; Ljungberg, M. P.; Wojdeł, J. C.; Íñiguez, J.; Rurali, R. A Phononic Switch Based on Ferroelectric Domain Walls. *Phys. Rev. B* **2017**, *96*, 140101(R).
(36) Liu, C.; Chen, Y.; Dames, C. Electric-Field-Controlled Thermal Switch in Ferroelectric Materials Using First-Principles Calculations and Domain-Wall Engineering. *Phys. Rev. Appl.* **2019**, *11*, 044002.
(37) Langenberg, E.; Saha, D.; Holtz, M.; Wang, J.; Bugallo, D.; Ferreiro-Vila, E.; Paik, H.; Hanke, I.; Ganschow, S.; Muller, D. A.; Chen, L. Q.; Catalan, G.; Domingo, N.; Malen, J.; Schlom, D. G.; Rivadulla, F. Ferroelectric Domain Walls in $PbTiO_3$ Are Effective Regulators of Heat Flow at Room Temperature. *Nano Lett.* **2019**, *19* (11), 7901–7907.
(38) Theis, C. D.; Schlom, D. G. Cheap and Stable Titanium Source for Use in Oxide Molecular Beam Epitaxy Systems. *J. Vac. Sci. Technol. A Vacuum, Surfaces, Film.* **1996**, *14*, 2677–2679.
(39) Smith, E. H.; Ihlefeld, J. F.; Heikes, C. A.; Paik, H.; Nie, Y.; Adamo, C.; Heeg, T.; Liu, Z. K.; Schlom, D. G. Exploiting Kinetics and Thermodynamics to Grow Phase-Pure Complex Oxides by Molecular-Beam Epitaxy under Continuous Codeposition. *Phys. Rev. Mater.* **2017**, *1*, 023403.
(40) Theis, C. D.; Schlom, D. G. The Reactivity of Ozone Incident onto the Surface of Perovskite Thin Films Grown by MBE. In *High Temperature Materials Chemistry IX*; Spear, K. E., Ed.; Electrochemical Society, Pennington, 1997; pp 610–616.
(41) Nair, H. P.; Liu, Y.; Ruf, J. P.; Schreiber, N. J.; Shang, S. L.; Baek, D. J.; Goodge, B. H.; Kourkoutis, L. F.; Liu, Z. K.; Shen, K. M.; Schlom, D. G. Synthesis Science of $SrRuO_3$ and $CaRuO_3$ Epitaxial Films with High Residual Resistivity Ratios. *APL Mater.* **2018**, *6*, 046101.
(42) Vlooswijk, A. H. G.; Noheda, B.; Catalan, G.; Janssens, A.; Barcones, B.; Rijnders, G.; Blank, D. H. A.; Venkatesan, S.; Kooi, B.; De Hosson, J. T. M. Smallest 90° Domains in Epitaxial Ferroelectric Films. *Appl. Phys. Lett.* **2007**, *91*, 112901.
(43) Catalan, G.; Lubk, A.; Vlooswijk, A. H. G.; Snoeck, E.; Magen, C.; Janssens, A.; Rispens, G.; Rijnders, G.; Blank, D. H. A.; Noheda, B. Flexoelectric Rotation of Polarization in Ferroelectric Thin Films. *Nat. Mater.* **2011**, *10*, 963–967.
(44) Nesterov, O.; Matzen, S.; Magen, C.; Vlooswijk, A. H. G.; Catalan, G.; Noheda, B. Thickness Scaling of Ferroelastic Domains in $PbTiO_3$ Films on $DyScO_3$. *Appl. Phys. Lett.* **2013**, No. 103, 142901.
(45) Kittel, C. Physical Theory of Ferromagnetic Domains. *Rev. Mod. Phys.* **1949**, *21*, 541–583.
(46) Mitsui, T.; Furuichi, J. Domain Structure of Rochelle Salt and KH_2PO_4. *Phys. Rev.* **1953**, 193–202.
(47) Roitburd, A. L. Equilibrium Structure of Epitaxial Layers. *Phys. status solidi* **1976**, *37*, 329.

(48) Pertsev, N. A.; Zembilgotov, A. G. Energetics and Geometry of 90°domain Structures in Epitaxial Ferroelectric and Ferroelastic Films. *J. Appl. Phys.* **1995**, *78*, 6170–6180.
(49) Schilling, A.; Adams, T. B.; Bowman, R. M.; Gregg, J. M.; Catalan, G.; Scott, J. F. Scaling of Domain Periodicity with Thickness Measured in $BaTiO_3$ Single Crystal Lamellae and comparison with other ferroics. *Phys. Rev. B* **2006**, *74*, 024115.
(50) Feigl, L.; McGilly, L. J.; Setter, N. Superdomain Structure in Epitaxial Tetragonal PZT Thin Films under Tensile Strain. *Ferroelectrics* **2014**, *465*, 36–43.
(51) Hsu, W. Y.; Raj, R. X-Ray Characterization of the Domain Structure of Epitaxial Lead Titanate Thin Films on (001) Strontium Titanate. *Appl. Phys. Lett.* **1995**, *67*, 792–794.
(52) Pompe, W.; Gong, X.; Suo, Z.; Speck, J. S. Elastic Energy Release Due to Domain Formation in the Strained Epitaxy of Ferroelectric and Ferroelastic Films. *J. Appl. Phys.* **1993**, *74*, 6012–6019.
(53) Zhang, Q.; Xie, L.; Liu, G.; Prokhorenko, S.; Nahas, Y.; Pan, X.; Bellaiche, L.; Gruverman, A.; Valanoor, N. Nanoscale Bubble Domains and Topological Transitions in Ultrathin Ferroelectric Films. *Adv. Mater.* **2017**, *29*, 1702375.

Table of Contents Graphic (TOC)